Electron Cyclotron Current Drive and Suprathermal Electron Dynamics in the TCV Tokamak

S. Coda 1), S. Alberti 1), P. Blanchard 1), T.P. Goodman 1), M.A. Henderson 1), P. Nikkola 1), Y. Peysson 2), O. Sauter 1)

1) Centre de Recherches en Physique des Plasmas, Association EURATOM-Confédération Suisse, Ecole Polytechnique Fédérale de Lausanne, CRPP - EPFL, CH-1015 Lausanne, Switzerland
2) Département de Recherches sur la Fusion Contrôlée, Association EURATOM-CEA, CEA/Cadarache, 13108 Saint Paul-lez-Durance Cédex, France

e-mail contact of main author: stefano.coda@epfl.ch

Abstract - Electron cyclotron current drive (ECCD) is an important prospective tool for tailoring the current profile in next-step devices. To fill the remaining gaps between ECCD theory and experiment, especially in the efficiency and localisation of current drive, a better understanding of the physics of suprathermal electrons appears necessary. On TCV, the fast electron population is diagnosed by a multichordal, spectrometric hard X-ray camera and by a high field side ECE radiometer. The main modeling tool is the quasilinear Fokker-Planck code CQL3D, which is equipped with a radial particle transport model. Systematic studies of fast electron dynamics have been performed in TCV with modulated or pulsed electron cyclotron power, followed by coherent averaging, in an attempt to identify the roles of collisional relaxation and radial diffusion in the dynamics of the suprathermal population. A consistent picture is beginning to emerge from experiment and modeling, pointing to the crucial role of the radial diffusion of suprathermal electrons in the physics of ECCD.

1. Introduction

Electron cyclotron current drive (ECCD) is an important tool for current profile shaping in magnetically confined plasmas, thanks to the highly localised power deposition of the EC wave and the ease of external control of its deposition location and wave-number spectrum. The strong influence exerted in turn by the current profile shape on the stability of the plasma to MHD modes, as well as on its confinement properties, motivates much current ECCD research.

The development of high power, high frequency, long pulse gyrotron sources in recent years has provided the fusion community with a versatile and mature technology for next-step thermonuclear fusion devices. The TCV tokamak (R=0.88 cm, a=0.25 cm, I_p<1 MA, B_T<1.54 T) is equipped with a 4.5 MW EC heating system, powered by six second harmonic (X2, 82.7 GHz) and three third harmonic (X3, 118 GHz) 0.5 MW gyrotrons. An extremely flexible EC beam delivery system, allowing real-time poloidal and toroidal steering, matches the equally flexible plasma position and shape control system of TCV [1].

ECCD experiments have been performed in TCV with the X2 system, for a total delivered power of up to 2.8 MW in X-mode, in a wide variety of plasma shapes, with a broad range of parallel wave numbers and heating locations. In particular, steady-state, fully non-inductive discharges sustained entirely by ECCD and bootstrap current are now routine on TCV [2-4].

The high energy electron population created by ECCD is diagnosed primarily with a hard X-ray (HXR) pinhole camera, on loan from Tore Supra, and with a high field side electron cyclotron emission (ECE) system. HXR bremsstrahlung emission is detected by a linear array of CdTe detectors along 14 chords which cover the outboard half of the cross section. The radial resolution is ~2 cm on the midplane, and the energy resolution is ~7 keV [5]. Spectral pulse height

analysis is performed with eight energy bins available for each chord, with adjustable thresholds within the 10-200 keV range.

The second harmonic X-mode ECE radiometer observes the plasma along one of three possible horizontal viewlines, two on the high field side and one on the low field side, and operates in the 78-114 GHz range with 24 channels of 0.75 GHz bandwidth [6]. The EC radiation observed on the high field side is dominated by relativistically downshifted emission by the high energy end of the electron distribution function and can thus be employed to diagnose the suprathermal population.

The quasilinear Fokker-Planck code CQL3D [7] is employed to model the dynamics of the electron distribution function. The code is coupled to the TORAY-GA ray-tracing module [8] and solves the Fokker-Planck equation in two velocity and one spatial dimensions. The equation includes a quasilinear EC wave damping term, a relativistic collision operator and a model for radial diffusion, with an optional linear dependence on the parallel velocity and a particle-conserving advection term.

2. ECCD and suprathermal electrons

The ability to control the deposition location and toroidal injection angle accurately is instrumental in the application of ECCD to current profile tailoring. This high degree of control was clearly demonstrated in TCV by sustaining the non-inductive plasma current with two X2 gyrotrons at the time, and firing two sets of two gyrotrons in succession for their maximum pulse durations (2 s). As shown in Fig. 1, the TCV discharge length was thus extended to a record 4.3 s, well beyond the maximum length achievable in Ohmic conditions. Matching the powers, deposition locations and parallel wave numbers of the two sets of beams is essential for a smooth switch-over. This external control was further demonstrated by an interlaced square-wave modulation of the two clusters (180 degrees out of phase), with no visible resulting modulation of the plasma parameters.

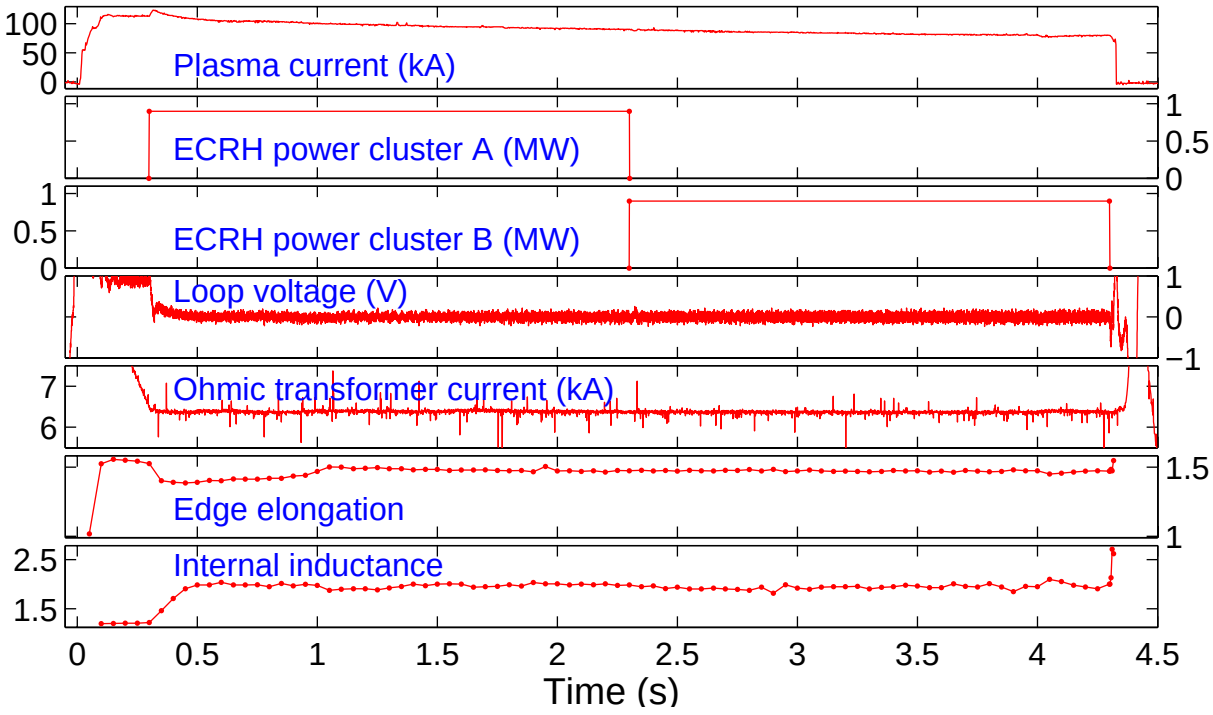

FIG. 1. TCV discharge 20881 of record length (4.3 s), sustained by 0.9 MW ECCD.

Current drive by electron cyclotron waves is theoretically predicted to operate on electrons traveling at substantially suprathermal velocities. Experimental measurements have confirmed that ECCD is accompanied by the creation and sustainment of a significant suprathermal population. Unmistakable suprathermal features are observed when the EC toroidal injection angle ϕ is nonzero, as required for ECCD: the HXR spectral distribution deviates from that of a Maxwellian plasma, and both the HXR photon temperature and the ECE radiative temperature are well in excess of the bulk plasma temperature measured by Thomson scattering [6,9,10]. By contrast, with $\phi \sim 0$ (pure heating mode) the three temperatures coincide.

The presence of a suprathermal electron population created by X2 ECCD has also been shown to engender enhanced absorption of the X3 waves over that expected for a Maxwellian plasma [11].

The energy resolved HXR measurement is a particularly sensitive indicator of the relative dynamics of the thermal and suprathermal components. In a series of recent experiments, an electron internal transport barrier (eITB) has been generated in a fully non-inductively driven plasma by applying off-axis co-ECCD at approximately mid-radius [12]. The barrier forms on a resistive diffusion time scale and is attributed to negative magnetic shear in the core. Once the barrier is formed, ECH power applied in the center increases both the energy and the confinement itself on a confinement time scale. Figure 2 clearly shows the distinct dynamics of the high and low energy components of the bremsstrahlung emission: the former originates from the suprathermal electron population, excited by the initial ECCD but essentially unaffected by the subsequent central ECH, whereas the latter is related to the temperature of the bulk population, which increases dramatically when central heating is applied.

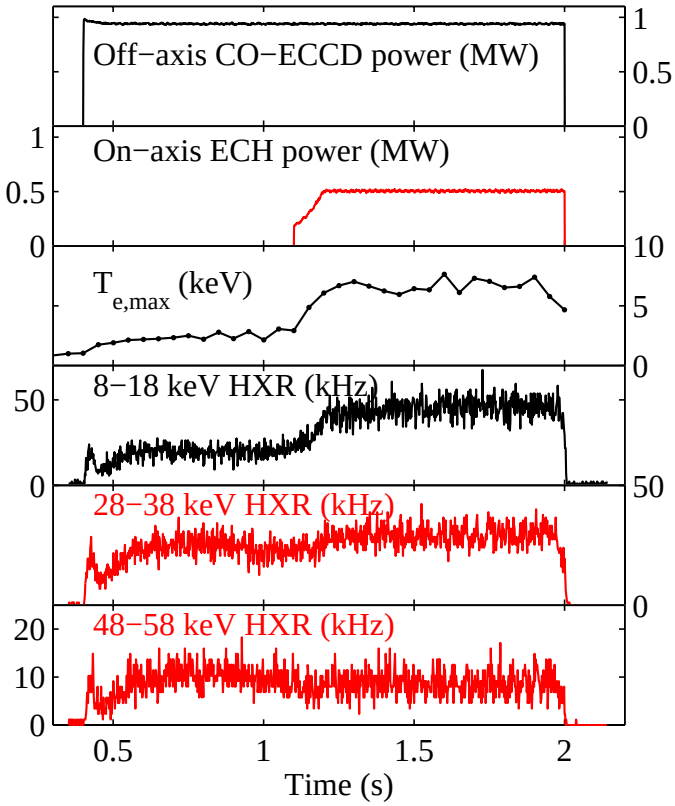

FIG. 2. Creation of an eITB with off-axis co-ECCD (TCV shot 22017). The traces shown are the powers of the two EC components, the peak electron temperature, and three energy channels of the HXR signal on a central chord.

The interpretation of ECE data is complicated by the fact that a given emission frequency corresponds to a continuum of spatial positions and electron energies, since the EC frequency depends, relativistically, on both magnetic field and energy. To deconvolve the two quantities some constraints must be applied. The approach that has shown the most promise is based on the assumption of a bi-Maxwellian electron distribution function, describing the bulk and suprathermal populations. This assumption is qualitatively supported by both HXR data and CQL3D modeling [6]. If profile shapes are assumed for the suprathermal density and temperature, the absolute values of these quantities can then be derived from the ECE data. A sensitivity study has shown that the final results do not depend strongly on the postulated profile shapes; canonical profiles have therefore been chosen, based on suggestions from the HXR data: in particular,

since the shape of the HXR spectrum is almost invariably independent of spatial location, it has appeared reasonable to assume a flat suprathermal temperature profile. If this procedure is correct, the derived suprathermal temperature should coincide with the HXR photon temperature (calculated from an exponential fit to the high energy component of the spectrum). Fair agreement has been found in the cases studied thus far. These results suggest that the suprathermal density can be up to 25% of the total electron density [6].

3. Suprathermal electron dynamics: the role of spatial diffusion in ECCD

The physical underpinnings of ECRH, particularly the absorbed power and the power deposition profile, have been validated by numerous experimental measurements [13]. Predictions for current drive have also been tested experimentally, with less uniform results: while good agreement with Fokker-Planck quasilinear theory is obtained in some devices [14], discrepancies remain in other cases. In particular, ECCD efficiency in TCV has been generally grossly overestimated by quasilinear theory, which predicted strong nonlinear enhancement by the unusually large EC power densities achieved. Linear theory, on the other hand, underestimates the driven current by factors ranging from 1 to 3.

The key to resolving these discrepancies appears to lie in the dynamics of the suprathermal electron population, as has been evidenced by CQL3D modeling of ECCD experiments. By including a diffusion coefficient D of the order of the bulk thermal diffusivity, the distribution of current-carrying fast electrons is broadened and nonlinear enhancement is strongly inhibited; with D~3 m^2/s, the experimentally measured EC-driven current can generally be reproduced. The same level of diffusivity does not change the predicted efficiency significantly in experimental situations in which nonlinear enhancement is not expected [15]. Thus a unifying picture is beginning to emerge.

The achievement of fully non-inductive discharges driven entirely by off-axis ECCD and bootstrap current, mentioned in the previous section, is a striking illustration of the effect of this suprathermal diffusivity. The value of D having been set such as to match the total driven current, the EC-driven current profile calculated by CQL3D is centrally peaked in spite of the power being deposited approximately at half-radius [16]. (It should be noted that the total current profile is nevertheless calculated to be hollow, owing to a large off-axis bootstrap current contribution.)

A direct experimental measurement of the spatial diffusivity presents formidable difficulties, as was already documented in the long history of lower hybrid current drive experiments [17]. The dynamics of suprathermal electrons are governed by several competing diffusive processes: collisional relaxation in velocity space (slowing-down and pitch-angle scattering), quasilinear rf diffusion in velocity space, and anomalous turbulence-driven diffusion in real space. There is no ‘source’ in the system, since the heating process itself is of a diffusive nature (albeit not energy conserving). Hence, several potentially overlapping time scales are at play, and an unambiguous determination of the complete system dynamics is difficult to conceive under controlled experimental conditions. On TCV, we have adopted the approach of applying multiple techniques aimed at providing progressively stronger constraints on these dynamics.

Two such techniques have been employed recently to exploit the specific characteristics of the HXR and ECE diagnostics, respectively. Square-wave modulation of the electron cyclotron power has been performed in order to enhance the photon statistics and thus the temporal resolution of the HXR camera by coherent averaging. Photon statistics also dictated high power lev-

els (typically 2.35 MW with 50% duty cycle), which resulted in strong modulation of the bulk plasma parameters, particularly density and temperature. Since the electron energy confinement time is of the same order as the slowing-down time for electrons travelling at 5 to 8 times the thermal velocity, a separation of the relevant time scales becomes impossible. However, information on the suprathermal dynamics is contained in the temporal evolution of the spectral distribution of the HXR signals. As mentioned in the previous section, the spectral shape in the relaxed state is nearly invariably uniform in space, even well outside the theoretical power deposition region. However, these measurements have shown for the first time that this is not the case immediately after switch-on: as shown in Fig. 3(a) for a case with central co-ECCD (ϕ=29^o), the signal from a central chord is initially larger than the off-axis signal at low energy, while their roles are reversed at high energy. The on-axis spectrum does not change appreciably over time, whereas the off-axis spectrum becomes similar to the former over a period of approximately 10 ms. A corresponding relaxation of the photon temperature profile towards a flat profile is seen in Fig. 3(b) [10].

The uniformity of the photon temperature suggests spatial equilibration. Electrons of different velocities are heated in different radial positions, owing to the Doppler shift required to match the local resonance condition in a spatially varying magnetic field. Additionally, the physical parameters that govern the steady-state distribution function, i.e. the EC power density, the bulk plasma density and the bulk electron temperature, are all spatially varying functions. Therefore the resulting spectral distribution should not be spatially uniform in general, unless communication is occurring over distant regions in space, i.e. by transport of suprathermal electrons. This evidence is considerably strengthened by the temporal evolution, which shows that the initial spectrum is indeed consistent with larger resonant velocities off-axis. From the observed relaxation time we can deduce a lower bound ~1.5 m^2/s for the diffusivity in this discharge.

The higher sensitivity of the ECE system is compatible with perturbative studies. In a second experiment, we have applied short periodic ECCD pulses to the plasma and studied the ECE response by coherent averaging. Pulses longer than 0.3 ms were seen to result in a first peak,

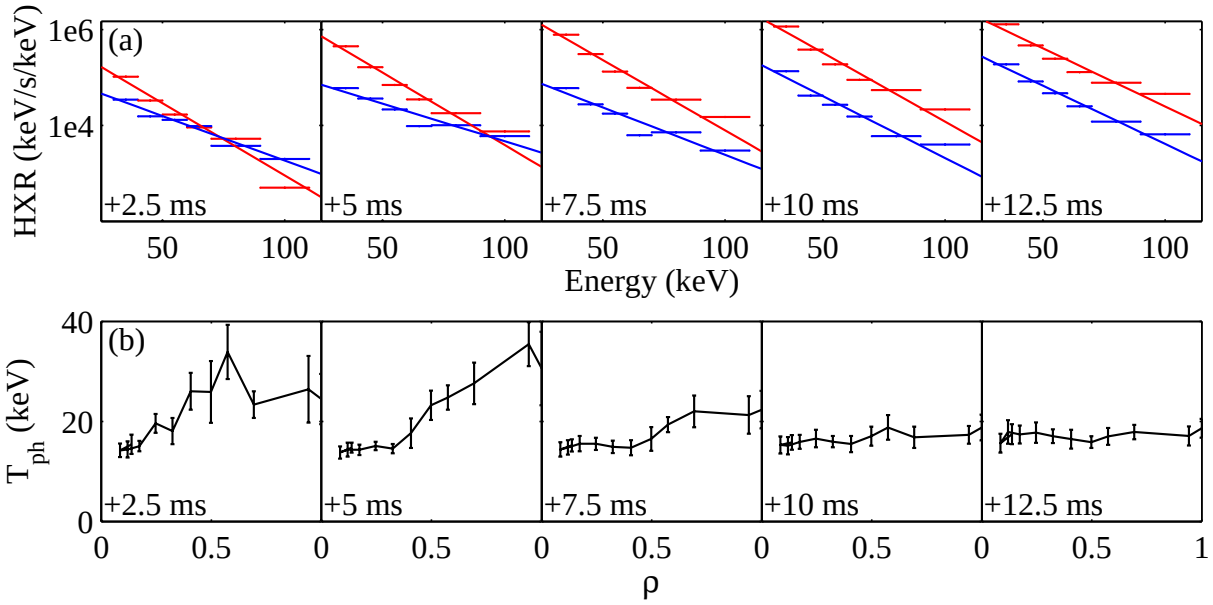

FIG. 3. TCV shot 21978: (a) HXR emissivity as a function of energy in 5 snapshots after the ECCD switch-on (t=0), for a central (red) and an off-axis (blue, ρ~0.6) chord; (b) spatial profiles of the photon temperature for the same snapshots (ρ here indicates the minimum normalized radius for each chord, i.e. the point of tangency to the flux surface) [10].

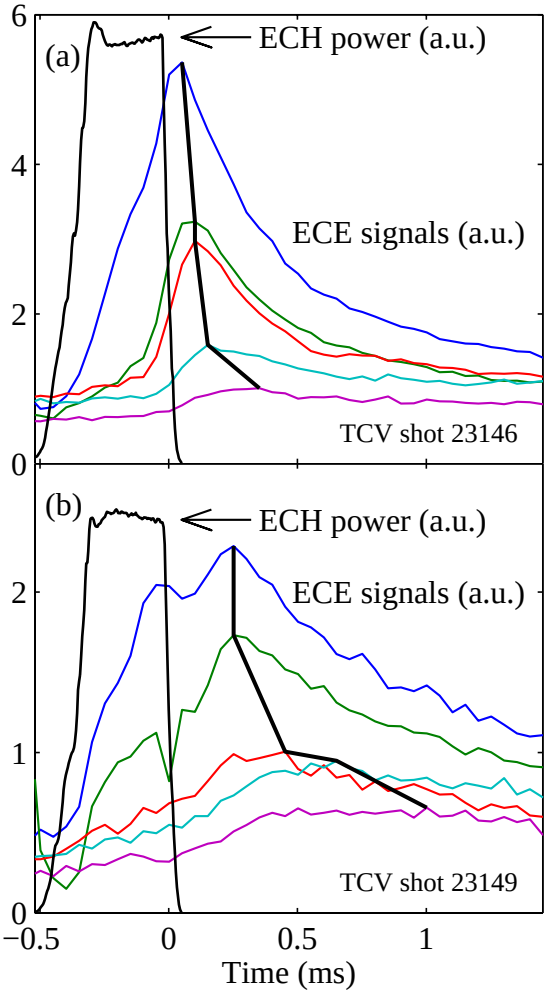

FIG. 4. Response of selected ECE signals to a short central ECCD pulse, averaged over 170 coherent pulses; the ECE frequency increases as the peak moves to later times; (a) ECE radiometer on the midplane, (b) ECE radiometer off-axis (ρ > 0.55). (See geometry in Fig. 5.)

followed by a descent and a further increase until the end of the pulse, indicating that the pulse length exceeded the characteristic rf diffusion time. To avoid this complicating effect, the pulse was thus kept to a length of 0.25-0.3 ms. The applied power was 0.45-0.9 MW with a period of 10 ms, therefore a 3% duty cycle and an average power < 27 kW, too low to affect the plasma parameters measurably. Two examples, both with central ECCD, are shown in Fig. 4, with the plasma and ECE radiometer geometries shown in Fig. 5. In the case of Fig. 4(a) the ECE chord goes through the plasma center, whereas in the case of Fig. 4(b) the smallest normalized minor radius accessed by ECE is approximately 0.55. In both cases the time to peak increases with the ECE frequency, as shown in Fig. 6. Moreover, the time lags are clearly larger when the ECE radiometer is aimed off-axis: indeed, when plotted versus the cold-resonance minor radius, the two curves connect smoothly to each other [Fig. 6(II)]. It should be remembered that an increase in frequency can be associated either to a shift towards the high field side (larger minor radius) or to an increase in electron energy; however, for equal energy and frequency, the signals from the two chords originate in different spatial regions. Thus this observation corroborates the hypothesis that a diffusive mechanism is at play and that a non-negligible fraction of the fast electrons generated by ECCD is transported far from the deposition region. A more quantitative analysis will require modeling. In particular, the time lag will generally depend on both the slowing-down time and the diffusion time: therefore the detailed dependence of the time lag on the frequency cannot uniquely provide quantitative information on the diffusion coefficient. The time to peak is, however, only one parameter of the dynamical response. The full dynamics, particularly the decay time, can provide strong constraints on the modeling. Further work is planned in this direction.

A further approach to studying the suprathermal electron relaxation phenomena consists of direct comparisons of HXR data with bremsstrahlung emission predicted by the CQL3D code for the specific geometry of our diagnostic. Without spatial diffusion, not only is the predicted current much too large, the predicted HXR signal is also far narrower spatially than the measured one. After the diffusion coefficient is adjusted to permit the code to match the total driven current, the results for the HXR emission are in much better agreement [10,15,18], generally within a factor of 3 everywhere, as exemplified by Fig. 7(a). In particular, these results provide strong evidence that the spatial uniformity of the spectral shape is a consequence of spatial transport. The shape is parametrized in Fig. 7(b) by a photon temperature, which is seen to be a strong function of minor radius in the case D=0, whereas with D=3 m^2/s a uniform temperature is recovered, which is moreover in very good quantitative agreement with the experimental values.

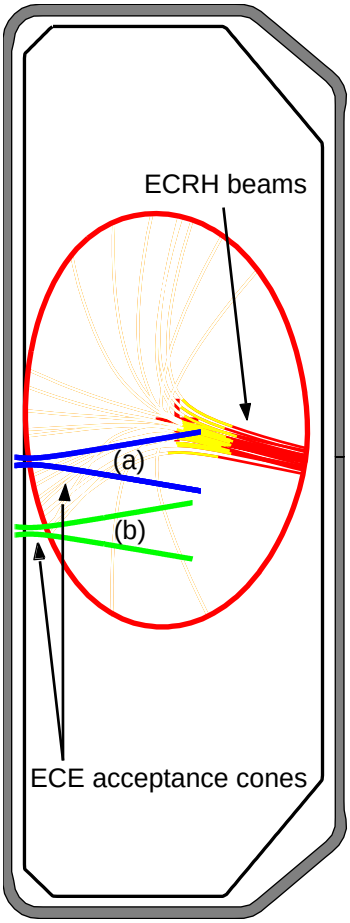

FIG. 5. Geometries of ECRH launching and ECE radiometry for the two cases shown in Fig. 5 (in reality the radiometer is fixed and the plasma and EC beams are moved).

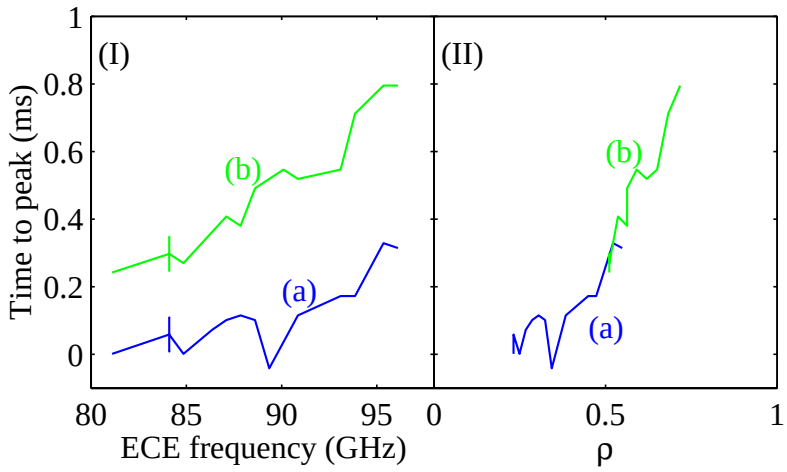

FIG. 6. Time lag from the end of the ECCD pulse to the ECE peak, for the two cases shown in Fig. 4, (I) as a function of ECE frequency, (II) as a function of the cold-resonance normalized radius.

It should be noted that the spectra are only approximately exponential; in particular, at higher energy the calculated slope in the diffusionless case becomes less steep (higher temperature) at larger radius.

4. Conclusions and outlook

ECCD is being used on TCV as a powerful tool for current and pressure profile shaping, especially with the high degree of control afforded by fully non-inductive operation, thus in the absence of an electric field, in steady state. At the same time, TCV is one of the premier test beds for fundamental inquiries into the physics of ECCD and the associated suprathermal electron dynamics, owing to a uniquely powerful and flexible ECH system and dedicated diagnostics, complemented by an advanced and flexible Fokker-Planck quasilinear code. The fundamental relaxation processes governing the suprathermal dynamics are being investigated through multiple experimental approaches and comparisons with modeling.

While strong evidence supports the conclusion that the suprathermal electrons excited by ECCD undergo cross-field diffusion at a rate comparable to that of thermal transport, much remains to be known about the dominant transport mechanism. Fokker-Planck simulations using different transport models, based on both electrostatic and electromagnetic turbulence, have thus far been inconclusive. A crucial question that must be addressed is the dependence of this transport on the ECH power density itself; it is plausible for instance to suppose a power degradation mechanism to be at play as in thermal transport, but this hypothesis has not yet been tested.

Acknowledgments

We are grateful to CEA-Cadarache for the loan of the hard X-ray camera and associated equipment, and to the entire TCV team for the operation of the tokamak and of the auxiliary heating systems. This work was supported in part by the Swiss National Science Foundation.

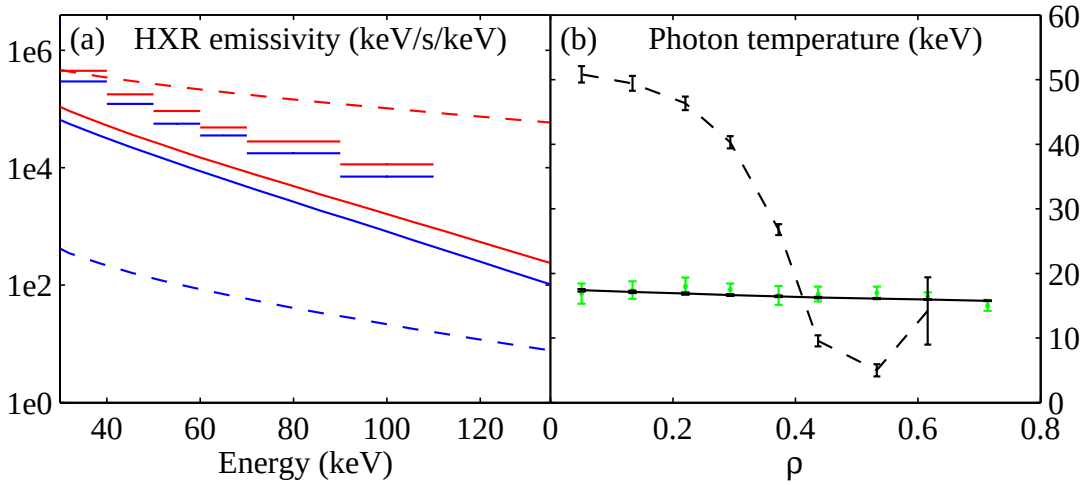

FIG. 7. TCV shot 21982: (a) HXR emissivity spectrum for a central chord (red) and a chord with a minimum ρ~0.37 (blue): experimental data (horizontal bars), CQL3D calculations with diffusivity D=3 m^2/s (solid lines) and D=0 (dashed lines); (b) photon temperature calculated from an exponential fit to the spectra in the interval 30-120 keV, as a function of radial position ρ (minimum normalized radius for each chord): experimental data (green), CQL3D data with D=3 m^2/s (solid black line) and D=0 (dashed black line).

References

[1] GOODMAN, T.P., et al., this conference (paper OV/4.2).
[2] SAUTER O., et al., Phys. Rev. Lett. **84** (2000) 3322.
[3] CODA S., et al., Plasma Phys. Control. Fusion **42** (2000) B311.
[4] SAUTER O., et al., Phys. Plasmas **8** (2001) 2199.
[5] PEYSSON Y., CODA S., IMBEAUX F., Nucl. Instrum. and Methods in Phys. Res. A **458** (2001) 269.
[6] BLANCHARD P., et al., Plasma Phys. Control. Fusion **44** (2002) 2231.
[7] HARVEY R.W., MCCOY M.G., in Proc. IAEA TCM/Advances in Simulation and Modeling in Thermonuclear Plasmas, Montreal (1992).
[8] MATSUDA K., IEEE Trans. Plasma Sci. **PS-17** (1989) 6.
[9] CODA S., et al., Proc. 26th EPS Conf. on Controlled Fusion and Plasma Physics (Maastricht 1999), Europhys. Conf. Abstr. **23J** (1999) 1097.
[10] CODA S., et al., Proc. 29th EPS Conf. on Controlled Fusion and Plasma Physics (Montreux 2002), Europhys. Conf. Abstr. **26B** (2002) (O-4.03).
[11] ALBERTI S., et al., Nucl. Fusion **42** (2002) 42.
[12] SAUTER O., et al., Proc. 29th EPS Conf. on Controlled Fusion and Plasma Physics (Montreux 2002), Europhys. Conf. Abstr. **26B** (2002) (P-2.087); GOODMAN T.P., et al., ibid. **26B** (2002) (p-2.081); SAUTER O., et al., this conference (paper EX/P5-06).
[13] See e.g. GOODMAN T.P., et al., Proc. 2nd Europhysics Topical Conf. on Radio Frequency Heating and Current Drive of Fusion Devices, Brussels, Belgium (1998), p. 245; PETTY C.C., et al., Strong microwaves in plasmas, vol. 1 (2000), p. 41.
[14] See e.g. PETTY C.C., et al., Nuclear Fusion **41** (2001) 551.
[15] HARVEY R.W., et al., Phys. Rev. Lett. **88** (2002) 205001.
[16] NIKKOLA P., et al., Proc. IAEA Tech. Committee Meeting on ECRH Physics and Technology for Fusion Devices and EC-12, Aix-en-Provence, France, 2002 (to be published).
[17] PEYSSON Y., Plasma Phys. Control. Fusion **35** (1993) B253.
[18] NIKKOLA P., et al., Proc. Joint Varenna-Lausanne Int. Workshop, Varenna, Italy, 2002, to be published in Theory of Fusion Plasmas (Editrice Compositori, Bologna, 2002).